Microstructure, topology and X-ray diffraction in Ag-metal reinforced polymer of polyvinyl alcohol of thin laminates

A. GAUTAM, P. TRIPATHY, S. RAM*
Materials Science Centre, Indian Institute of Technology Kharagpur, Kharagpur 721302, India
E-mail: sram@matsc.iitkgp.ernet.in

Published online: 12 April 2006

A polymer composite of Ag-metal reinforced polyvinyl alcohol (PVA) is synthesized in shape of thin laminates of 200–300 μm thickness. The process involves a chemical Ag^+ dispersion in PVA and in-situ $Ag^+ \rightarrow Ag$ reduction-reaction with active PVA molecules under hot conditions (with stirring) in water at 60–70°C temperature. The product results in a metal Ag-polymer complex dispersed in the solution. After evaporating part of water, a derived viscous solution is casted (in hot conditions) in shape of a thin laminate in a glass mould. In addition to chemical reducer, active OH-groups (free from H-bonding) in PVA molecules of refreshed surfaces act as head groups to adsorb Ag^+ and drive a directional $Ag^+ \rightarrow Ag$ growth. Short fibrils of Ag-metal thus occur in reaction over the PVA molecules. Casting thin laminates from a liquid sample Ag-PVA allows the fibrils (also the polymer molecules) to align along the surface. Selected Ag-contents up to 5.0 wt.% in Ag-PVA laminates are studied in terms of scanning electron micrograph, X-ray photoelectron spectroscopy (XPS) and X-ray diffraction. Average size, morphology and aspect ratio (φ) vary in Ag-metal depending on the Ag-content. As long Ag-metal fibrils as 2–5 μm, $\varphi = 35$, occur in a sample of 2.0 wt.% Ag. The Ag-metal reflects in two characteristic $3d_{5/2}$ and $3d/_{3/2}$ XPS bands of 368.3 and 374.1 eV respectively.

1. Introduction

Polyvinyl alcohol (PVA) offers a simple example to exploit as a polymer matrix for deriving a reinforced polymer composite with a filler of an immiscible metal such as copper, silver, or gold. Besides a readily available compound, PVA is soluble in water, which eases chemical mixing, dispersion and/or reaction of this kind of inorganic fillers with refreshed reactive PVA molecules (with OH-groups free from H-bonding) in aqueous medium. Different kinds of fillers [1–9] affect PVA matrix in different ways, resulting in unique dielectric, electrical, and optical properties, with superior thermal stability, useful for optical and electronic devices, catalysts, sensors, and other applications. It is shown that doped PVA by small particles due to Ag-metal behaves as a semiconductor [9, 10].

Devi et al. [10] studied electrical and optical absorption properties in silver nitrate (0.25–1.0 wt.%) doped PVA as films of thickness $t \sim 6.7$ μm. The doping was performing by mixing $AgNO_3$ into PVA at room temperature in water. The mixed solution was put as film in a sandwich configuration of Al-film-Al and then dried in a hot air for 24 h. The doping reflects in an increase in electrical conductivity σ by a factor as much as 10^5 at room temperature at an optimal 0.5 wt.% $AgNO_3$. The σ-value decreases at a larger doping concentration. An optical absorption band occurs at 413 nm due to the doping. Mbhele et al. [6] developed Ag-metal reinforced PVA nanocomposites by dispersing an Ag–metal colloid (deduced via a chemical Ag_2SO_4 reduction with $NaBH_4$ in water) in an aqueous PVA at room temperature. Composite films, $t \sim 400$ μm, of 0.19, 0.33 and 0.73 wt.% Ag (of 20 nm particles) were obtained of considerably improved thermal, mechanical and viscoelastic behaviors of virgin PVA films after evaporating the solvent in air at room temperature.

In another experiment, Feng et al. [7] prepared similar Ag-PVA films by mixing an Ag-metal colloid to PVA in water followed by casting a concentrated sample at room temperature. The Ag-metal colloid was deduced by reducing $AgNO_3$ with tannic acid and Na_2CO_3 in water.

*Author to whom all correspondence should be addressed.
0022-2461
DOI: 10.1007/s10853-006-6768-4

Near spherical or cubic shaped Ag–particles lie of 20–30 nm diameter. A contrary to the results of Devi et al. [10] of $AgNO_3$ doped PVA films, the σ-value had been found to be rather decreased by an order of magnitude on adding $\sim$0.03 wt.% Ag-metal of such small particles. Raising the Ag-content further results in no significant change in the σ-value. When metal nanoparticles are dispersed in insulator, the composite structure may assume adversely a decreased σ-value by the theory of Coulomb blockade [7, 11, 12].

In this article, we report novel results of microstructure and topology in Ag-PVA nanocomposites (0–5 wt.% Ag) of thin laminates. It is observed that, under hot conditions in water, Ag^+ cations react with PVA molecules, forming Ag-metal dispersed in a matrix of the PVA molecules. After evaporating part of solvent at elevated temperature, latter is casted in desired shape in a mould. Short fibrils of Ag-metal occur with part of PVA molecules to be aligned along the laminate surface. The results are analyzed in correlation of photoelectron spectroscopy (XPS) and X-ray diffraction (XRD) of selected samples.

2. Experimental details

2.1. Synthesis of $Ag^+ \rightarrow Ag$ species and Ag-PVA composite structure

A chemical dispersion and instantaneous reduction of Ag^+ cations to Ag-metal (as small particles) in a polymer matrix of dispersed PVA molecules in hot water are explored to synthesize Ag-metal (nanoparticles) doped PVA in an Ag – PVA composite structure. Doing the reaction (between Ag^+ cations and PVA molecules) with a continuous magnetic stirring (under hot conditions) refines PVA molecules of refreshed reactive surfaces in smaller PVA molecules, which serve as active reaction centres to operate a controlled $Ag^+ \rightarrow Ag$ reaction in divided reaction groups. The Ag-metal particles so obtained in this way keep to be embedded in a dispersed structure in polymer matrix of refined PVA molecules at out-set of the reaction. No separate Ag-metal synthesis is involved unlike in the earlier studies [6, 7]. The whole synthesis process is described as follows.

This simple reaction is carried out in single step with two simple starting chemicals of (i) a silver compound such as silver nitrate $AgNO_3$ and (ii) a polymer such as PVA. They dissolved easily in a common solvent of distilled water. Freshly prepared solutions in PVA (weight average molecular weight $\sim$125000) and $AgNO_3$ were used in predetermined ratios according to the final Ag-PVA compositions. Both the reagents were as pure as 99.9% (procured from the Aldrich Chemicals). A typical reaction batch of $AgNO_3$ of an initial 1.0 M concentration was used with a 3.0 g/dl PVA in deionized water in a total 250 ml volume. As given in Table I, six Ag-PVA reaction batches, involving 0–5.0 wt.% Ag-contents, were thus prepared under the common conditions of the initial concentrations and the total volume in the two reagents. Magnetic stirring under hot conditions at 60–70°C is used to obtain a colorless transparent PVA solution before adding the $AgNO_3$ to induce the $Ag^+ \rightarrow Ag$ reaction.

TABLE I. Experimental conditions for forming Ag^+ doped PVA polymer precursors and derived Ag-PVA composites of thin laminates

Ag-content (wt.%)	Volume (ml)		Monomer/Ag^+ ratio
	$AgNO_3$	PVA	
0	0	250.00	–
0.2	0.14	249.86	1218
0.5	0.35	249.65	487
1.0	0.70	249.30	243
2.0	1.40	248.60	121
5.0	3.50	246.50	48

A batch of 250 ml sample was taken in stoichiometric ratio in 1.0 M $AgNO_3$ and 3.0 g/dl PVA solutions.

When adding $AgNO_3$ to such a PVA-solution dropwise, under the heating conditions and the stirring, an instantaneous $Ag^+ \rightarrow Ag$ reaction occurs in presence of refined reactive PVA molecules. A colloid forms due to so obtaining Ag-metal of ultrafine particles and those being dispersing in PVA molecules divided in small Ag-PVA groups. Under these reaction conditions, the apparent colour in the resulting sample Ag-PVA (consists of derived Ag-metal nanoparticles, which are dispersed and embedded in the PVA polymer matrix) deepens gradually from an achromatic colour in the beginning to a faint yellowish to a brownish reddish (or blackish in the case of the Ag-rich compositions) equilibrium colour. Notice the final colour of Ag-PVA colloid depends sensitively on the experimental conditions of (i) the rate of $AgNO_3$ addition to aqueous PVA solution, (ii) the initial concentration in $AgNO_3$ or PVA solution, (iii) average temperature during mixing the two components, and (iv) the thermomechanical stirring process. These four basic experimental parameters govern the$Ag^+ \rightarrow Ag$ conversion process and dispersion of derived Ag-species in a complex structure in reactive PVA molecules.

In order to retain a stable Ag-PVA colloid structure, which consists of Ag-metal nanoparticles caped in PVA molecules of thin films or layers, the sample was cooled at 20–25°C temperature just after the reaction. The polymer surface layer of PVA molecules over such Ag-metal particles behaves to be rather stable on 20–30 h of aging at this temperature, i.e., far below the glass transition temperature T_g in virgin PVA [13, 14]. Otherwise, the PVA polymer layer piles off the Ag-metal surface and the latter often encounter agglomeration and growth into independent Ag-metal particles of irregular shapes. Finally, a concentrated sample is obtained by evaporating part of the water at the temperature 60–70°C as used during the primary reaction. As summarized in Fig. 1 a viscous Ag-PVA sample so obtained is casted in form of thin laminates in a mould of a silicate glass. Samples of 200–300 μm thickness occur after drying in air at room temperature. The Ag-PVA laminates of six selected compositions of

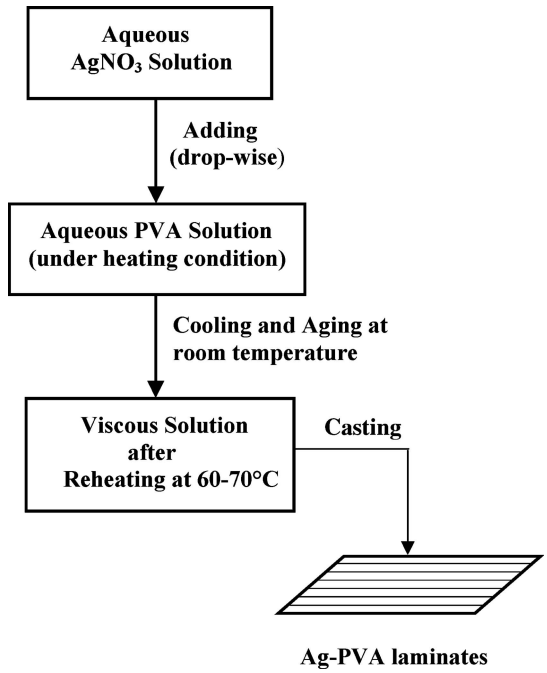

Figure 1 Schematic diagram of forming an Ag-PVA nanocomposite in shape of thin laminates following an $Ag^+ \rightarrow Ag$ chemical reaction and dispersion of derived Ag-metal nanoparticles over polymer molecules of PVA in deionized water under hot conditions.

0–5 wt.% Ag-contents (Table I) were prepared in this way. In ambient atmosphere, the thin laminates, especially containing the Ag-metal nanoparticles, behave to be better stable. Unlike bulk PVA, which is bit hygroscopic, no significant change occurs in mass or other properties in an extended period of exposure in dry air at room temperature.

2.2. Characterization of Ag-PVA composite structure

Microstructure and topology in thin laminates in Ag-PVA composites were studied with a scanning electron microscope (SEM) of JEOL model JSM-5800 (or Oxford model Leo1550). An energy depressive X-ray (EDX) spectrum analyzer, in conjunction with the SEM, was used for in-situ chemical analysis of the samples in selected regions. The XPS data were collected with help of a VG ESCALB MK–II spectrophotometer by exciting the sample (thin laminate) under a reduced pressure $\sim 10^{-8}$ Pa, with Mg $K\alpha_{1,2}$ radiation of $h\nu = 1253.6$ eV energy operating at 12 kV and 20 mA. Phase analysis is carried out with XRD patterns, which were recorded with a P.W. 1710 X-ray diffractometer using CuKα radiation of wavelength $\lambda = 0.15405$ nm.

3. Results and discussion

3.1. $Ag^+ \rightarrow Ag$ reaction and Ag-metal growth process over PVA molecules

According to the observation, the PVA molecules in this example serve three basic purposes of (i) a dispersoid, (ii) a chemical reducer, and (iii) a templateing agent. As a result, when adding $AgNO_3$ to a hot PVA solution in water, the metal cations Ag^+ disperse over refreshed reactive PVA molecular surfaces, and grow as Ag-metal with local reactions with the PVA molecules in specific shapes according to the local PVA structures. Under heating conditions in aqueous PVA at 60–70°C, the magnetic stirring causes a microstructure of refreshed reactive PVA molecules, with activated OH-groups free from H-bonding. In this experiment, the sample (in a beaker) rotates in concentric layers in a specific flow pattern according to the stirring process, vessel's shape and other conditions. Internal friction between PVA layers in relative motions refines the sample in small PVA molecules of thin laminates by a process of mechanochemical stretching. In extended stirring, those get to be as thinned as a molecular layer and disperse in the hot water.

The temperature during the stirring promotes local molecular dynamics so that small PVA molecules rearrange and retain in thin shapes of laminates. At a total of 3.0 g/dl content, in hot water, they disperse and dissolve easily in a transparent solution in a highly dispersed structure. Nevertheless, in no case, the local temperature exceeds average T_g-value, which lies in the 60–130°C range (230–260°C melting point) as per the PVA tacticity [13, 14]. This is important to retain the basic structural units or segments to be immobile in amorphous state. Otherwise, small laminates recombine one another in a complex structure, leaving behind no longer an effective value of active OH-groups.

As demonstrated in Fig. 2 in a model example, a thin PVA laminate has several active OH groups. They act as head-groups to adsorb Ag^+ cations (while adding $AgNO_3$) and lead to convert them into Ag^0, which ultimately grows as Ag-metal over the PVA surface. In Fig. 2a, >R–OH represents a PVA monomer. A reaction of it with Ag^+ can be expressed as follows:

$$\begin{aligned} &>\text{R–OH} + \text{Ag}^+ \rightarrow >\text{R–O–Ag} + \text{H}^+, \\ &>\text{R–O–Ag} \quad\;\; \rightarrow -\text{R=O} + \text{Ag}^0 \\ \hline &>\text{R–OH} + \text{Ag}^+ \rightarrow -\text{R=O} + \text{Ag}^0 + \text{H}^+. \end{aligned} \tag{1}$$

Here, "–R=O" represents a monomer in a partially oxidized PVA at the reaction surface while H^+ is an acid byproduct HNO_3. A characteristic C=O stretching band occurs in "–R=O" in infrared spectrum at 1730 cm^{-1}.

A simple model molecular structure in Fig. 2b in a thin laminate consists of interchain bridging between PVA molecules. This involves H-bonding in OH-groups from adjacent PVA backbone chains, forming a planar structure. Only two backbones are involved in this model in a simple case. It encounters several head-groups free from the H-bonding, especially at the chain borders. During the reaction, they add Ag^+ cations easily in a specific template structure along the laminate. A directional chemical

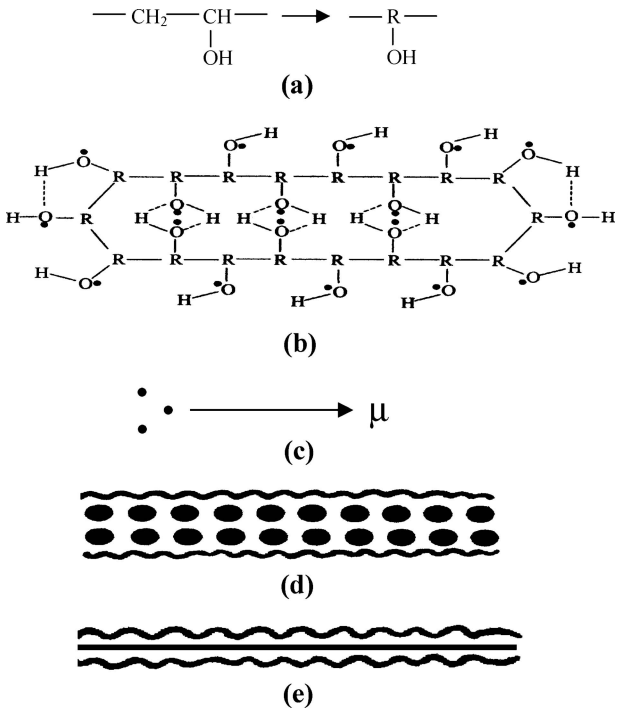

Figure 2 (a) PVA monomer, (b) a model planar template of PVA polymer molecule with Ag^+ cations (•) attached to OH^- groups in each of the monomers, (c) the local chemical potential μ, (d) the Ag-lattice patterning after a local reaction in Ag^+ and OH^- in template (b), and (e) a thin laminate or fibril shape of Ag-metal in the composite Ag-PVA (thin laminate).

potential μ sets-in and drives a directional $Ag^+ \rightarrow Ag - e^-$ reaction (Fig. 2c). It activates neighboring O–H groups to participate in a co-directional reaction by unbonding the H-bonds. The heat of the reaction, which flows primarily along the reaction surface in the local reaction centres, favors the directional reaction. As a result, Ag-species (Fig. 2d) grow as Ag-metal of fibrils or laminates (Fig. 2e) over the polymer surface. In a realistic case, in accordance to microstructure (Figs. 3–5) in the Ag-metal, a planar template extends over a rather large number (n) of linear PVA chains. A value of $n = D/M_w \sim 2 \times 10^3$ is obtained in a molecularly thin template of width $D \sim 1\ \mu$m, with a chain width $M_w \sim 0.5$ nm.

A linear or a thin planar structure of PVA often turns into a spiral shape [8, 14]. Also in this shape it templates (along length L) a directional $Ag^+ \rightarrow Ag - e^-$ reaction. Aspect ratio, $\varphi = L/B$, in derived Ag-metal particle (of width B) depends on initial φ-value in the template. It is quite likely that, during adding the Ag^+ species, weak $Ag^+ - PVA$ templates encounter to disintegrate in small pieces. As discussed in example of Zr^{4+} or Cr^{4+} [8, 15, 16], a miceller structure occurs of capping Ag^+ species in PVA molecules. This occurs in optimizing the total surface energy in resulting shapes according to thermodynamics of reaction species [8, 15, 17]. As evident with microstructure (Fig. 4), in this specific case, the $Ag^+ \rightarrow Ag^0$ species grow within the micelle in a spherical shape.

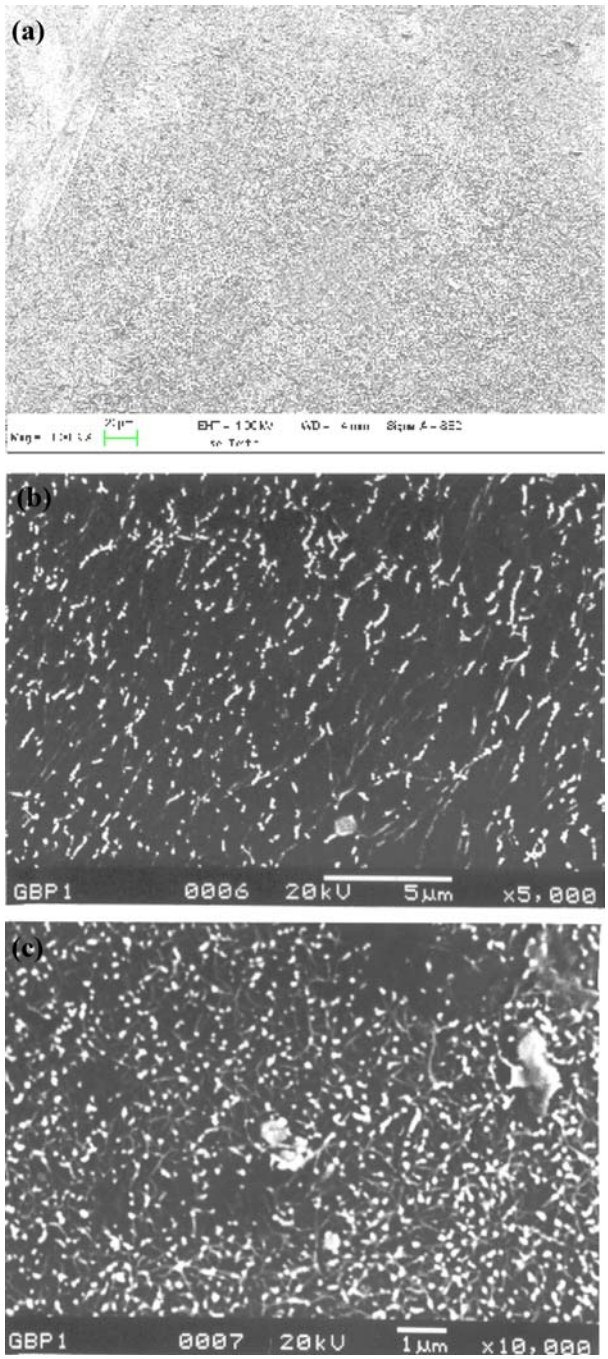

Figure 3 SEM micrographs in Ag-PVA nanocomposites of thin laminates; (a) 0.0, (b) 0.5, and (c) 1.0 wt.% Ag-contents.

3.2. Microstructure and topology in Ag-PVA composites

Fig. 3 compares SEM images in (a) a pure and (b) 0.5 or (c) 1.0 wt.% Ag doped PVA of thin laminates. Features (of a whitish contrast) have developed on inclusion of the Ag-metal contents. A careful observation at a glance reveals nearly spherical or platelet shapes of images (particles), which are aligned in elongated shapes. In fact, small particles have morphology of a rectangular slab (prism), with a cross section view of a thin platelet of

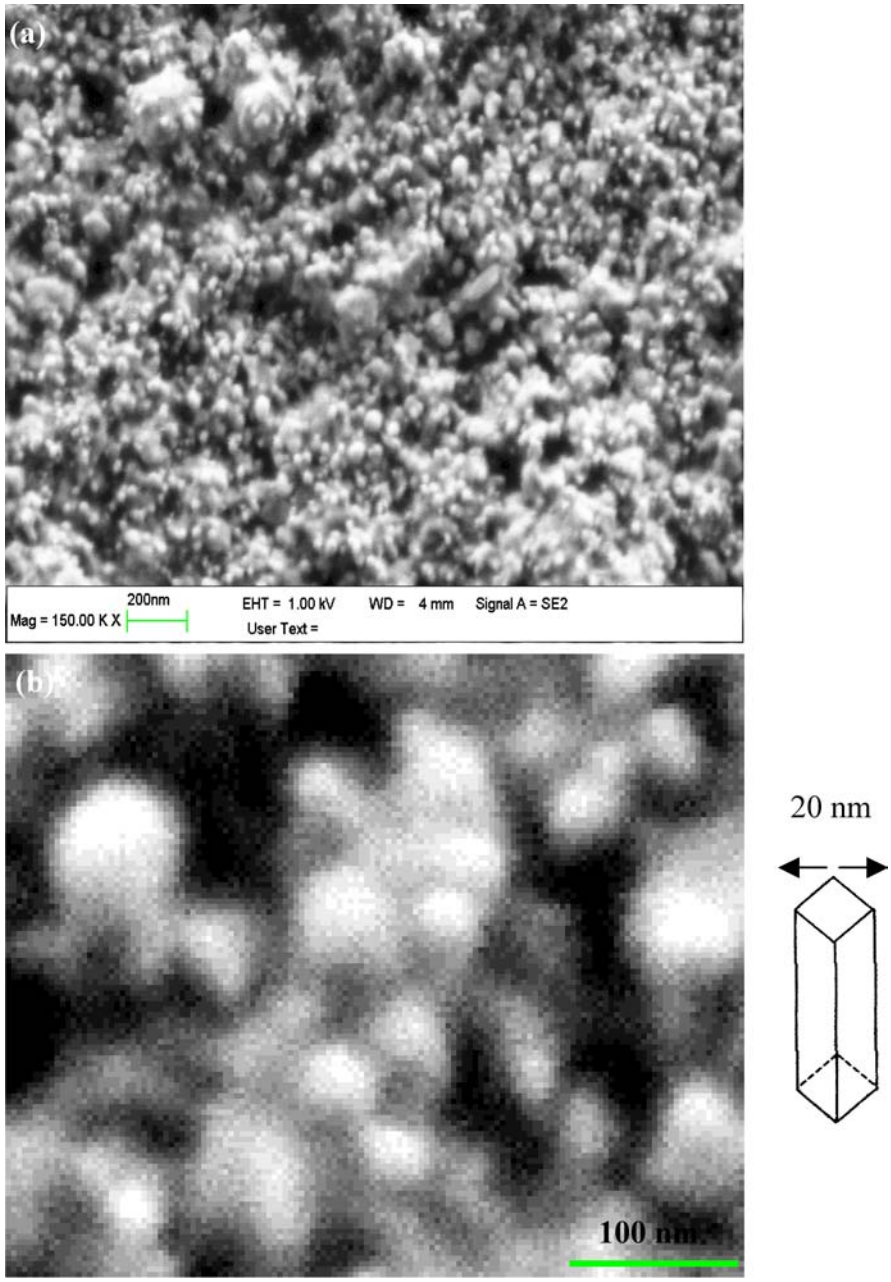

Figure 4 (a) High-resolution SEM images showing prismatic shapes of Ag-metal, with a thin capping surface layer of PVA polymer, in 1.0 wt.% Ag-PVA nanocomposite of thin laminate. (b) A close-up of the prismatic shapes with a model one in the right.

a rectangular or square shape, as in a tetragonal lattice. The particles facing-up with square cross section along the surface under the SEM observation reflect in a cubic or nearly spherical shape. A rectangular shape of cross section reflects in other orientations.

In order to analyze shapes in such particles further, we studied SEM images at a higher resolution. A typical micrograph is shown in Fig. 4a for a 1.0 wt.% Ag-PVA sample. A fairly sharp size distribution lies of distinct particles. Most of them are of a square or rectangular shape of cross sections, with an average 20 nm diameter. In-situ EDX analysis confirms that they are due to Ag-metal, which is embedded in a PVA polymer matrix. A close-up of part of such images is given in Fig. 4b. It very much demonstrates presumably prismatic shapes of Ag-crystallites. Average width β lies at a scale of $\sim$20 nm (represents effective crystallite size) in 20–50 nm long crystallites. Polymer coats the crystallites making difficult to get their virginal images. A model shape of crystallites is included in the right to the SEM images in Fig. 4b.

Well-defined fibrils of Ag-metal occur in raising the Ag-contents in the 2–5 wt.% range. As can be seen from SEM in Fig. 5a, as long fibrils as $\sim$25 μm appear, with average $B = 0.5$ μm value ($\varphi \sim 40$), in an optimal 2.0 wt.% Ag-content. Most of them consist of acicular particles ($L = 2$–5 μm and $B = 0.5$ μm) aligned as clusters in this specific shape of fibrils, which lie along surface of the sample

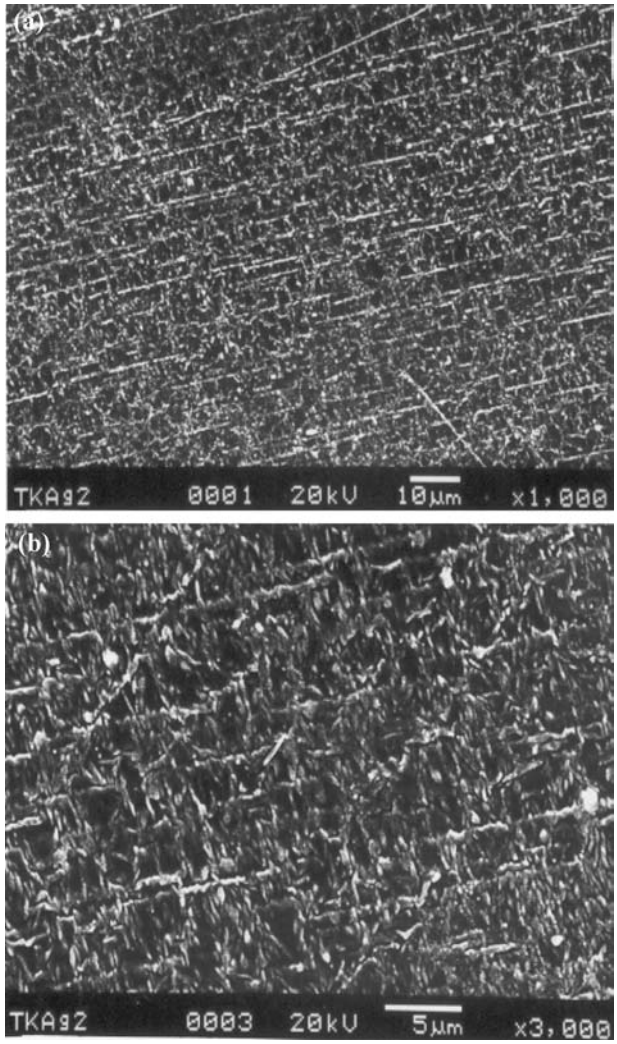

Figure 5 (a) SEM images of mostly short fibrils and (b) a close-up of acicular or oval shaped particles in the fibrils in 2.0 wt.% Ag-PVA nanocomposite of thin laminate.

(thin laminate). In a close-up of micrograph in Fig. 5b, similar acicular particles, which lie in other orientations to the sample surface, reflects apparently in smaller sizes in part of the cross sections under the observation. Small particles are interbridging or cross-linking fibril structures in a web-like structure. It occurs through PVA molecules, which embed the Ag-particles in such shapes. This is important for deriving thermal stability and other improved properties in a hybrid Ag-PVA composite structure.

A further increase in Ag-metal content to 5.0 wt.% results in rather small fibrils (Fig. 6a or b) of $L = 2$–3 μm, $B = 0.2$ μm, and $\phi \sim 2$–3. They are clusters (as illustrated with a model structure in Fig. 6) of Ag-metal crystallites. High-resolution SEM images (Fig. 6c) reveal distinct crystallites ($\beta \sim 35$ nm). Obviously, the initial Ag^+-content in the reaction influences the nucleation and growth of final Ag-metal crystallites. Larger the Ag^+-content larger is the effective β-value. A furthermore, in this reaction, the formation of Ag-metal, which occurs over dispersed PVA molecules in solution, leads the

TABLE II. Average length L, width B, aspect ratio φ, crystallite size β, volume fraction of whitish contrast F_c, and morphology in clusters in Ag-PVA composites of thin laminates

Ag-content (wt.%)	L (nm)	B (nm)	φ	β (nm)	F_c (%)	Morphology
0.0	–	–	–	–	05	No distinct shape
0.2	20–40	15—25	1–2	15	10	Fibrils
0.5	20–50	20—30	1–5	20	15	Fibrils
1.0	20–50	20—30	1–2	20	25	Laminates
2.0	2000–5000	500	40	25	35	Fibrils
5.0	2000–3000	200	2–3	35	45	Fibrils

A deep-whitish contrast lies of Ag-metal particles while the matrix phase lies in light-whitish contrasts of PVA disintegrated in small structures.

PVA to disintegrate into smaller molecules. Refined PVA molecules no longer support a nondisrupted Ag-metal growth in so extended shapes of fibrils as observed from the microstructure. The values of L, B, φ and β obtained in clusters in Ag-metal (or PVA) in the various samples are given in Table II. An analysis of the SEM images of whitish contrasts gives a larger value of volume fraction F_c (Table II) than expected in the Ag-metal in part of recrystallized or disintegrated PVA in small structures.

A prismatic or cubiod shape is not common in such small Ag-metal particles [6, 7, 18–21]. Ag-PVA nanocomposites (0.19–0.73 wt.% Ag) derived from dispersing an Ag–metal colloid in aqueous PVA have spherical particles of ~ 20 nm diameter [6]. The result is consistent with the present work that Ag-metal crystallites have similar size, but in anisotropic shape of thin prisms. Difference lies in two independent reactions and/or mixing procedures used in the two examples. In the chemical method used here, an Ag^+ templateing with planar PVA molecules initiate and drive an anisotropic nucleation and growth of Ag-metal over the $Ag^+ \rightarrow Ag$ reaction surface, which consists of PVA molecules in the template in part of the reaction.

3.3. X-ray diffractograms in Ag-PVA composites

XRD patterns are studied of thin Ag-PVA laminates (200–300 μm thickness) to analyze phase of Ag-content in terms of crystalline structure. In principle, in this example, it could occur and exist as a pure metal as well as an oxidized metal Ag_2O after reaction of $AgNO_3$ with active PVA molecules as discussed above. The analysis demonstrates that a presumably metallic phase occurs of small crystallites as follows.

In XRD (Fig. 7 or 8), new peaks occur in weak intensities on 1.0–5.0 wt.% Ag-doping in PVA. Strong XRD background accompanies the diffractogram in characteristic reflection from an amorphous structure in part of the PVA polymer matrix. That masks weak crystalline peaks difficult to resolve and analyze their features. The amorphous phase is characterized with two diffraction halos in two primary pair distribution functions of the C, O

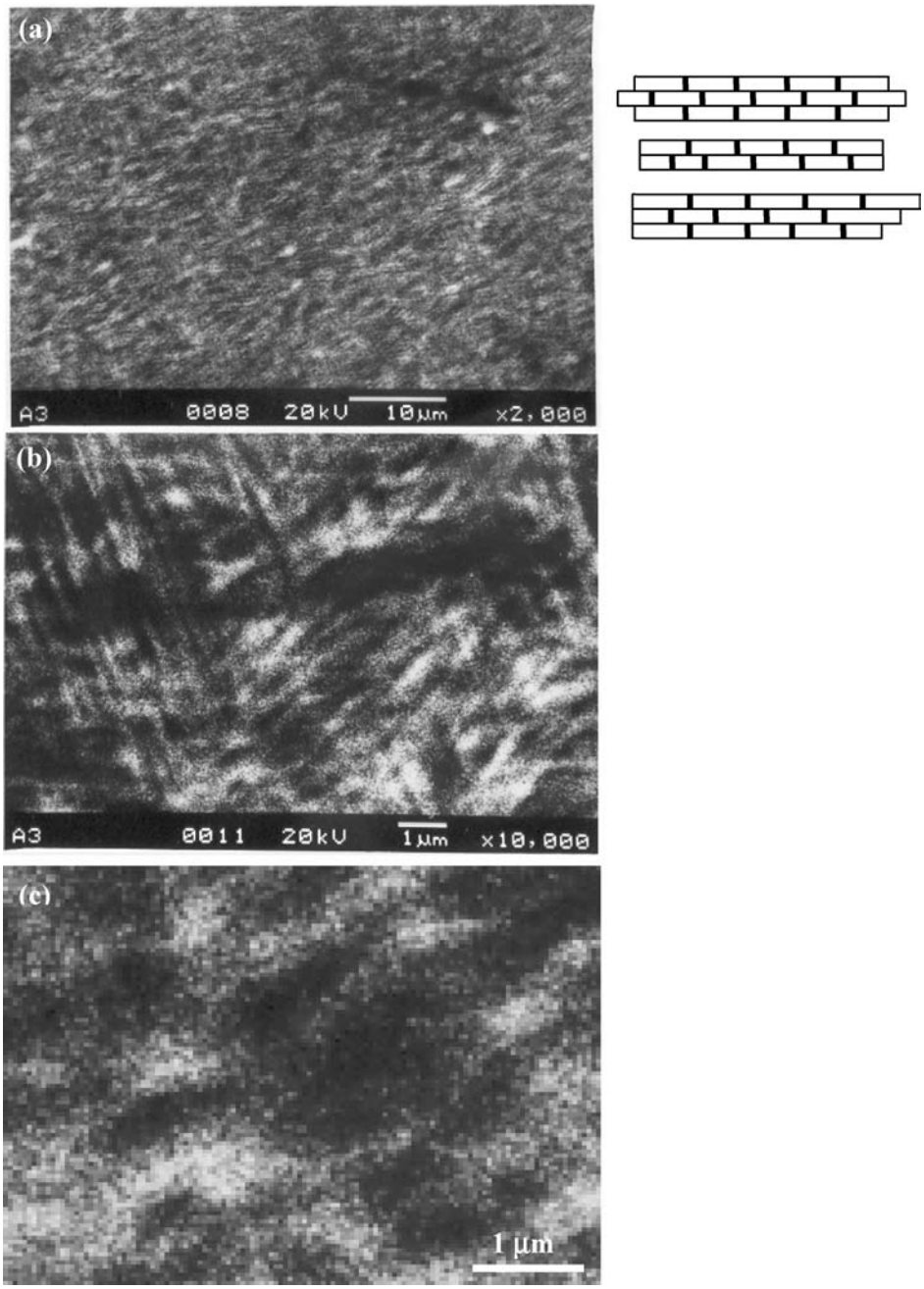

Figure 6 SEM images in (a) short fibrils and (b) acicular or oval shaped particles (as shown with the models in the right) in 5.0 wt.% Ag-PVA nanocomposite of thin laminate. (c) A close-up showing basic fibril components of thin laminates (a tetragonal lattice).

and H constituent atoms [8, 15]. They lie at wavevectors $q_1 = 13.6$ and $q_2 = 28.1$ nm^{-1} in pure PVA-films (Fig. 7a). A similar diffractogram lies of $q_1 = 12.0$ and $q_2 = 28.2$ nm^{-1} in the starting PVA powder used to obtain the films [8, 15]. Further modified halos lie of $q_1 = 13.9$ and $q_2 = 27.6$ nm^{-1} in the 2.0 wt.% Ag or $q_1 = 14.2$ and $q_2 = 27.8$ nm^{-1} in the 5.0 wt.% Ag contents.

In the Ag-PVA films, two diffraction halos encounter a regular decrease in peak intensity (I_p) as a function of the Ag-content. Halo q_1 has a value of $I_p = 87, 70$ and 42 units in the 1.0, 2.0 and 5.0 wt.% Ag-contents, respectively, relative to an $I_p = 100$ units value in virgin PVA films. In Ag-PVA films, it is quite likely that the PVA occurs in thin layers along the film surface. A collective reflection of the X-ray beam (used to measure the XRD) from these layers occurs in an intense (also rather sharpened) diffractogram q_1. An average $\Delta r \sim 0.45$ nm separation (which is comparable to the M_w value) is determined between the layers from the q_1-value. The results infer that the formation of Ag-metal crystallites, which occurs in support over PVA molecules, promotes in return a devitrification or disintegration of PVA in small structures. In SEM, such refined PVA structures reflect in relatively enriched whitish contrasts but not so opaque as in the case of the Ag-metal

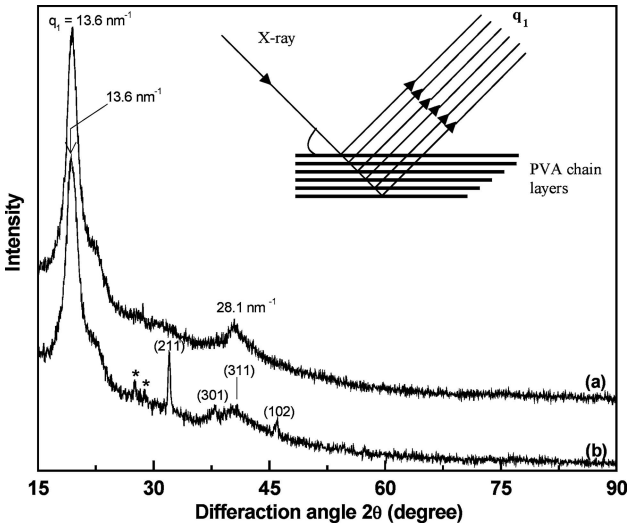

Figure 7 X-ray diffractograms in (a) the virgin PVA and (b) 1.0 wt.% Ag-PVA nanocomposite of thin laminates. Reflection from PVA in thin layers is shown in the in-set. * Not identified.

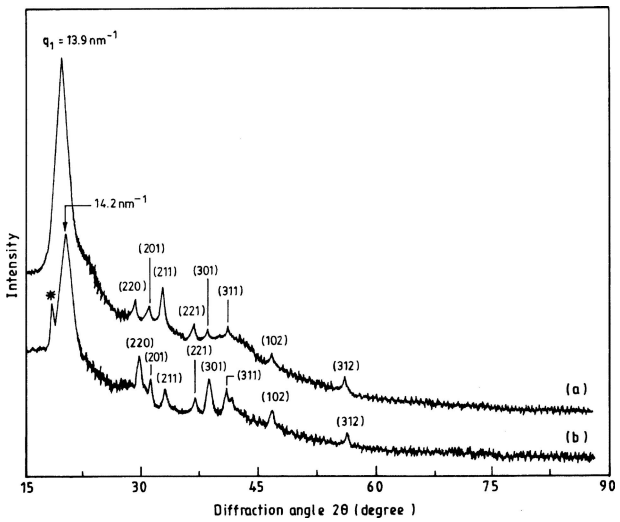

Figure 8 X-ray diffractograms in Ag-PVA nanocomposite of thin laminates; (a) 2.0 and (b) 5.0 wt.% Ag-contents. * Not identified.

particles. This is the reason that the SEM images measure a larger value of whitish contrasts F_c than expected in the Ag-metal particles alone (Table II).

Interplanar spacings d_{hkl} and relative intensities I_p in XRD peaks observed in Ag-PVA of 1.0, 2.0 and 5.0 wt.% Ag are given in Table III. No such peaks occur in distinct intensities at lower Ag-contents. The present values of d_{hkl} and/or I_p differ from the values in well-known Fm3m cubic and $P6_3/mmc$ hexagonal Ag-metal crystal structures [21–23]. No d_{hkl} value lies above 0.2359 nm in the fcc-Ag (Table IV). Oxidized Ag-metal as Ag_2O characterizes a different pattern [21, 22]. As a noble metal, under hot conditions, as used here, it hardly encounters oxidation so easily. In Table III, the d_{hkl} values are reproduced, within a standard deviation of $\pm$ 0.002 nm, assuming a tetragonal structure of lattice parameters $a = 0.8505$ and $c = 0.4120$ nm.

TABLE III. Interplanar spacings (d_{hkl}) and relative intensities (I_p) in X-ray diffraction peaks in Ag-metal in thin Ag-PVA laminates

1.0 wt.% Ag		2.0 wt.% Ag		5.0 wt.% Ag					
d_{hkl} (nm)	I_p	d_{hkl} (nm)	I_p	d_{hkl} (nm)	I_p	Calculated (d)	h	k	l
0.3230	25								
–		0.3025	75	0.3005	100	0.3009	2	2	0
–		0.2940	65	0.2935	60	0.2957	2	0	1
0.2790	100	0.2800	100	0.2785	70	0.2793	2	1	1
–		0.2445	50	0.2440	55	0.2428	2	2	1
0.2360	15	0.2345	45	0.2340	90	0.2335	3	0	1
0.2250	20	0.2240	45	0.2240	55	0.2252	3	1	1
0.1970	15	0.1995	30	0.1990	20	0.1998	1	0	2
–		0.1635	25	0.1630	15	0.1635	3	1	2

The I_p values, reported after subtracting the background intensity I_b, are tentative only. Actual I_p values are not feasible to estimate in the predominant I_b –value.

TABLE IV. Interplanar spacings and relative intensities in X-ray diffraction peaks in Ag-metal in Fm3m cubic crystal structure

d_{hkl} (nm)	I_p	h	k	l
0.2359	100	1	1	1
0.2044	40	2	0	0
0.1445	25	2	2	0
0.1231	26	3	1	1
0.1180	12	2	2	2
0.1022	04	4	0	0
0.0938	15	3	3	1
0.0914	12	4	2	0
0.0834	13	4	2	2

The lattice parameter $a = 0.40862$ nm and density $\rho = 10.50$ g/cm^3 (after ref. [22]).

Details of structures in three Ag-allotropes are given in Table V. The Ag-metal in this example of $Ag^+ \rightarrow Ag$ reaction grows in the structure, which provides a similarity with the initial templateing structure with the PVA molecules. Over an extended planar PVA surface (Fig. 2), Ag-metal thus nucleates and grows initially in a thin laminate structure, with atomic packing primarily along the surface. This is satisfied with a kind of a tetragonal lattice, which involves the unit cell of a thin laminate shape, with a-value as large as 2.06 times the c-value. A hexagonal unit cell could offer another preferred structure of growth,

TABLE V. Lattice parameters, lattice number Z, lattice volume V_0, aspect ratio, and density ρ in Ag-metal in three allotropes

Allotrope	Z	Lattice parameters (nm)	V_0 (nm^3)	Aspect ratio	ρ (g/cm^3)	Ref.
Cubic	4	$a = 0.4086$	0.0682	1.00	10.50	[22]
Hexagonal	4	$a = 0.2886$ $c = 1.0000$	0.2164	3.46	9. 93	[22]
Tetragonal	16	$a = 0.8505$ $c = 0.4120$	0.2980	0.48	9.61	Present work

The aspect ratio is taken as the ratio in c and a-values.

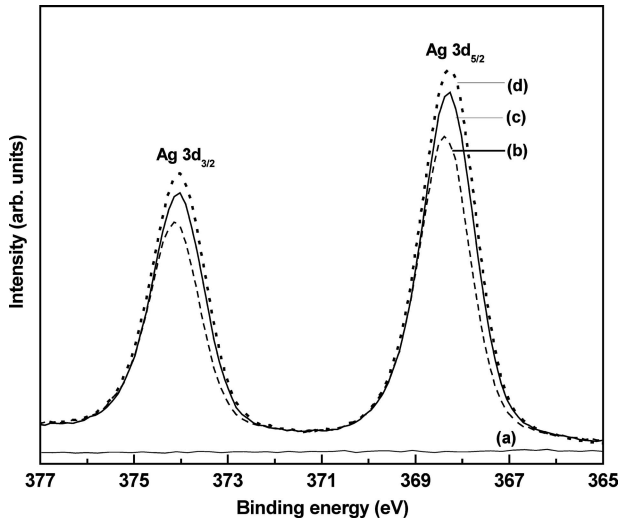

Figure 9 XPS spectra in $3d_{5/2}$ and $3d_{3/2}$ Ag bands in Ag-PVA nanocomposite of thin laminates; (a) 0, (b) 0.2, (c) 0.5, and (d) 1.0 wt.% Ag-contents.

if grows with *c*-axis (*a*-axis in the present example) along the template, under the influence of a similar $c/a \cong 3.46$ value. An isotropic shape of crystallites, as in the otherwise common fcc-Ag phase, is not favorable to grow in support with the anisotropic templates in this example.

3.4. XPS bands in Ag-metal crystallites in Ag-PVA composites

The XPS spectrum in Ag-PVA composites is used to confirm valence state of the silver and to comment on the effects of PVA polymer matrix on the Ag-electronic structure in terms of the binding energies E_b and/or half-bandwidths ΔE_b in the characteristic bands. It is a very sensitive analytical tool for this kind of studies in pure elements, compounds, or composites in crystalline, amorphous, or other states [24–29]. For example, Fig. 9 compares XPS spectra, in the 365–377 eV range, for (a) 0, (b) 0.2, (c) 0.5, and (d) 1.0 wt.% Ag in the Ag-PVA composites. No XPS bands lie in PVA in this range. As given in Table VI, a well-resolved double structure occurs with 368.3 and 374.07nbsp;eV of E_b values in the two components. The separation in two bands is $\Delta E_d \sim 5.7$ eV irrespective to the Ag-contents. In bulk Ag-metal, they lie at 368.3 and 374.3 eV [24, 28]. The results confer that the total Ag-content exists in the valence state of pure metal

TABLE VI. Band positions E_b, relative intensities (I_p) and bandwidths (ΔE_b) in XPS bands in Ag-metal in Ag-PVA composites of thin laminates

Ag-content (wt.%)	Ag $3d_{5/2}$ band			Ag $3d_{3/2}$ band		
	E_b (eV)	(I_p)	ΔE_b (eV)	E_b (eV)	(I_p)	ΔE_b (eV)
0.2	368.39	37	1.20	374.15	28	1.22
0.5	368.26	41	1.22	374.03	31	1.24
1.0	368.25	44	1.24	374.02	33	1.25
5.0	368.37	100	1.25	374.13	73	1.26

TABLE VII. Average E_b values in $3d_{5/2}$ and $3d_{3/2}$ bands in Ag^0 and Ag^+ states in bulk Ag-metal, Ag-nanoparticles, surface passivated Ag-nanoparticles, Ag-clusters, Ag-PVA composites, and Ag_2O metal oxide

Sample	E_b-value (eV)		ΔE_d (eV)	Ref.
	$3d_{5/2}$ band	$3d_{3/2}$ band		
Bulk Ag-metal	368.3	374.3	6.0	[24, 28]
Ag-Nanoparticles (12 nm)	368.8	374.9	6.1	[28]
N-passivated Ag-nanoparticles*	367.7	–		[26]
Ag-metal clusters	368.8	–		[24]
0.5 wt.% Ag-PVA composite	368.3	374.0	5.7	Present work
0.5 wt.% Ag-PS composite*	369.5	375.3	5.8	[27]
0.5 wt.% Ag-AS composite*	369.7	375.7	6.1	[27]
Ag_2O metal oxide	368.0	374.0	6.0	[28]

*N: 1-Nonanethiol, PS: polystyrene copolymer and AS: Acrylonitrile-styrene copolymer.

Ag^0. A change of $Ag^0 \rightarrow Ag^+$ results in a marginally lowered E_b value, e.g., 368.0 and 374.0 eV in the two bands in Ag_2O [25 , 28].

A comparison of the data in Table VII infers that Ag-nanoparticles have an increased E_b-value over the bulk value, e.g., the $3d_{5/2}$ band has shifted from 368.3 eV of the bulk value to a value of 369.7 eV. A surface polymer coating of Ag-particles, or a reinforcing of Ag-particles in a polymer matrix in a composite structure, causes a further modification in E_b values according to interactions between the two phases. The shift in the E_b-value can be attributed to five major effects: (i) charging, (ii) effective particle or crystallite size, (iii) crystal structure, (iv) chemical bonding with the surroundings, and (v) interparticle interactions. The effects (i) result from the creation of $Ag \rightarrow Ag^+$ species at the Ag-particle surface. In the kinds of the composites Ag-PVA, it accompanies a ligand $\rightarrow$ metal (or vice-versa) charge transfer, depending on the ligand (here PVA). As the particle size decreases, the electronic structure changes in a way of increasing the bandgap E_p or the E_b-value, as observed in particles of size under 12 nm.

In the Ag-PVA samples, an adversely decreased E_b value in $3d_{5/2}$ and $3d_{3/2}$ Ag-bands is possible in predominating involvements of the last two effects. The Ag-particles, which are caped in thin PVA surface layers, no longer encounter as strong interparticle interactions (improves E_b value) as in a single component sample of Ag-nanoclusters or nanoparticles. In another example, a mesoporous ZrO_2 offers a satellite band of $E_b = 174.3$ eV [16], i.e. smaller even to the Zr^0 value 178.5 eV [30, 31], to the main $3d_{5/2}$ or $3d_{3/2}$ Zr^{4+} band of 182.7 or 184.7 eV. This signal arises in reduced interparticle interactions via mesopores. A lower atomic packing density in the tetragonal structure, relative to the fcc-Ag (Table V), has another input to decrease E_b value. A decrease of E_b-value correlates to a concomitant increase in the σ-value,

i.e., as much as a factor of 10^3, as a function of the doping to 1–2 wt.% Ag [9, 10]. Systematic studies of electrical conductivity, optical absorption, and other band structure derived properties are demanded before to comment on involvements of E_b in the individual factors.

4. Conclusions

In hot conditions (60–70°C), $AgNO_3$ reacts with PVA (polyvinyl alcohol) molecules in water, forming a metal Ag-polymer complex, which is dispersed in the PVA polymer. PVA of refreshed molecular surfaces, in process of the reaction, offers active OH-groups (free from the H-bonding) to serve as head groups to operate the $Ag^+ \rightarrow Ag - e^-$ reaction. This occurs in support over molecular PVA surfaces. Ultimately, Ag-metal nanoparticles nucleate and grow in specific crystal structure and morphology according to the polymer template structure. Evaporating part of water results in a viscous Ag-PVA gel, which is casted and dried in shape of thin laminates (200–300 μm thickness) at room temperature. A composite structure persists in Ag-contents up to 5.0 wt.% as the filler.

As studied with SEM images, the Ag-metal nanocrystallites occur in groups (clusters) in shapes of fibrils, which lie along the sample surface. Casting a liquidus Ag-PVA with H_2O in a thin laminate leads the Ag-metal particles to align along with part of PVA molecules in fibril structures embedded in the PVA polymer. It occurs according to the surface anisotropy and flow of the heat (during the cooling) along the surface. In increasing Ag-content, Ag-crystallite size grows hardly from 15 nm at 0.2 wt.% to 35 nm at 5.0 wt.% Ag. As long Ag-PVA fibrils as 2–5 μm occur, with aspect ratio $\varphi = 35$, in the sample of an optimal 2.0 wt.% Ag.

According to the X-ray diffractogram, Ag-crystallites in thin Ag-PVA laminates grow in shape of a crystal unit cell that is derived from the laminate structure in a structural similarity to the template with PVA molecules. A tetragonal crystal structure of an extended a-value, i.e. about twice the a-value in the bulk fcc-Ag, thus occurs. XPS analysis ensures the Ag-contents to be present in the valence state of pure metal Ag^0. The Ag-crystallites embedded in PVA polymer represent a good example of a dispersed structure of metal particles in a dilute dielectric system. As a consequence, the 3d Ag XPS bands in Ag-PVA composites have a decreased value of the binding energy, by as much as 0.9 eV, relative to the value in a single-phase sample of Ag-nanoparticles or clusters alone.

Acknowledgments

The authors gratefully acknowledge the Council of Scientific and Industrial Research (CSIR), Government of India, and the Ministry of the Human Resource and Development (MHRD), Government of India, for the financial supports

References

1. M. S. P. SCHAFFER and A. H. WINDLE, *Adv. Mater.* **11** (1999) 937.
2. R. V. KUMAR, Y. KOLTYPIN, Y. S. COHEN, D. AURBACH, O. PALCHIK, I. FELNER and A. GEDANKEN, *J. Mater. Chem.* **10** (2000) 1125.
3. D. Y. GODOVSKY, *Adv. Polym. Sci.* **153** (2000) 165.
4. X. F. QIAN, J. YIN, J. C. HUANG, Y. F. YANG, X. X. GUO, and J. K. ZHU, *Mater. Chem. Phys.* **68** (2001) 95.
5. Y. H. YU, C. Y. LIN, J. M. YEH, and W. H. LIN, *Polym.* **44** (2003) 3553.
6. Z. H. MBHELE, M. G. SALEMANE, C. G. C. E. VAN SITTRET, J. M. NEDELJKOVIC, V. DJOKOVIC and A. S. LUYT, *Chem. Mater.* **15** (2003) 5019.
7. Q. FENG, Z. DANG, N. LI and X. CAO, *Mater. Sci. and Eng. B.* **99** (2003) 325.
8. S. BISWAS and S. RAM, *Chem. Phys.* **306** (2004) 163.
9. A. GAUTAM, S. RAM and S. K. ROY, Proceeding of Intern. Symposium on Advance Materials and Processing, Edited by Adhikari, Banthia, Basu, Bhargava, Jacob and S Ram, (Cygnus Advertising Press, 2004) p 1386.
10. C. U. DEVI, A. K. SHARMA and V. V. R. N. RAO, *Mater. Lett.* **56** (2002) 167.
11. J. H. F. SCOTT-THOMAS, S. B. FIELD, M. A. CASTNER, H. I. SMITH and D. A. ANTONIADIS, *Phys. Rev. Lett.* **62** (1989) 583.
12. D. Y. GODOVSKI, *Adv. Polym. Mater. Sci. Eng.* **72** (1995) 283.
13. J. H. CHOI, S. W. KO, B. C. KIM, J. BLACKWELL and W. S. LYOO, *Macromolecules* **34** (2001) 2964.
14. S. RAM and T. K. MANDAL, *Chem. Phys.* **303** (2004) 121.
15. S. RAM, *J. Mater. Sci.* **38** (2003) 643.
16. A. MONDAL and S. RAM, *Chem. Phys. Lett.* **382** (2003) 297.
17. S. RAM, *Acta. Mate* . **49** (2001) 2297.
18. A. HENGLEIN and M. GIERSIG, *J. Phys. Chem. B* **103** (1999) 9533.
19. Y. SUN, Y. YIN, B. T. MAYERS, T. HERRICKS and Y. XIA, *Chem. Mater.* **14** (2002) 4736.
20. B. YIN, H. MA, S. WANG and S. CHEN, *J. Phys. Chem. B* **107** (2003) 8898.
21. H. WANG, X. QIAO, J. CHEN and S. DING, *Colloidal Surf. A: Physicochem. Eng. Aspects* **256** (2005) 111.
22. X-ray Powder Diffraction File JCPDS-ICDD (Joint Committee on Powder Diffraction Standard-International Centre for Diffraction Data, Swarthmore, PA) (a) 04-0783, fcc-Ag, (b) 41-1402, hcp-Ag, (c) 75-1532, Pn3m-cubic Ag_2O, and (d) 76-1393, P3m-cubic Ag_2O.
23. M. ZHENG, M. GU, J. JIN and G. JIN, *Mater. Res. Bull.* **36** (2001) 853.
24. G. K. WERTHEIM, S. B. DICENZO and D. N. E. BUCHANAN, *Phys. Rev. B* **33** (1986) 5384.
25. J. C. R. C. KING, JR., *Handbook of X-ray Photoelectron Spectroscopy* (Physical electronics Inc., Eden Prairie, Minnesota, 1992) p. 121.
26. S. HE, J. YAO, S. XIE, S. PANG and H.GAO, *Chem. Phys. Lett.* **343** (2001) 28.
27. R. ZENG, M. Z. RONG, M. Q. ZHANG, H. C. LIANG and H. M. ZENG, *Appl. Surf. Sci.* **187** (2002) 239.
28. H. S. SHIN, H. C. CHOI, Y. JUNG, S. B. KIM, H. J. SONG and H. J. SHIN, *Chem. Phys. Lett.* **383** (2004) 418.
29. S. RANA, S. RAM, S. SEAL and S. K. ROY, *Appl. Surf. Sci.* **236** (2004) 141.
30. M. MATASUOKA, S. ISOTANI, S. MIYAKE, Y. SETSUHARA, K. OGATA and N. KURATANI, *J. Appl. Phys.* **80** (1996) 3109.
31. W. WANG, H. T. GUO, J. P. GUOR, X. H. DONG and Q. X. QIN, *J. Mater. Sci.* **35** (2000) 1495.

Received 9 May
and accepted 1 September 2005